


Mode-superposition-induced transparency

Khoa V. Bui  and A. T. Rosenberger *

Department of Physics, Oklahoma State University, Stillwater, Oklahoma 74078, USA

 (Received 16 February 2022; accepted 29 August 2022; published 9 September 2022)

Induced transparency in a microresonator can result from cross-polarization coupling of two coresonant orthogonally polarized whispering-gallery modes of very different Q . The coupling creates supermodes that are superpositions of the two modes. In this paper we show that mode superpositions that result from simultaneous excitation of two orthogonally polarized modes can also show induced transparency, even in the absence of cross-polarization coupling. Induced transparency is accompanied by pulse delay, and it is also possible to observe induced attenuation with pulse advancement or delay. These effects are modeled, simulated numerically, analyzed theoretically, and confirmed experimentally. The results are presented here.

DOI: [10.1103/PhysRevA.106.033504](https://doi.org/10.1103/PhysRevA.106.033504)

I. INTRODUCTION

Polarization effects in whispering-gallery-mode (WGM) microresonators represent a topic of increasing interest and importance [1–6]. We have previously studied coupled-mode-induced transparency (CMIT) and Autler-Townes splitting (ATS) with pulse delay, and coupled-mode-induced attenuation (CMIA) with pulse advancement or delay, when there is coupling between two coresonant modes that have very different quality factors (Q s) and orthogonal polarizations [7–9]. These behaviors may be exploited for numerous applications such as signal processing and optical sensing [10–12].

In our earlier work [7–9], the mode coupling under study was cross-polarization coupling, resulting from the optical spin-orbit interaction. The interaction between the spin and extrinsic orbital angular momentum of light in a WGM causes a weak polarization rotation, resulting in cross-polarization coupling (CPC). This is made possible by slight axial asymmetry of the resonator, for example, a hollow bottle resonator. A difference in the effective indices of refraction of the coupled modes, one TE (transverse electric) and one TM (transverse magnetic), then results in their coupling being nonreciprocal [13].

If the CPC amplitudes are t_{21} for coupling from mode 1 (input) to mode 2 and $-t_{12}$ for 2 to 1 coupling (see Fig. 1), the destructive interference that gives CMIT comes from light coupled from 1 to 2 and back into 1, so that this contribution to the intracavity mode 1 field amplitude picks up a factor of $-T_c = -t_{21}t_{12}$, where T_c is the CPC strength. The mode coupling creates supermodes (analogous to the normal modes of coupled oscillators) that are linear superpositions of TE and TM.

The existence of these linear superpositions created by CPC led us to wonder what would happen in a system in which linear superpositions of coresonant TE and TM modes

resulted from a process other than mode coupling. The resulting investigation is reported here.

Again, the two modes will have very different Q s, but there is no CPC. The superposition is created by injecting light that is linearly polarized at 45° in the TM-TE (1-2) basis, simultaneously exciting both TE and TM modes. As in the CPC experiments, we detect the throughput light of the same polarization as the input, 45° . We find behavior qualitatively the same as in the CPC case, namely mode-superposition-induced transparency (MSIT) with pulse delay and mode-superposition-induced attenuation (MSIA) with pulse advancement or delay. (Since there is no TM-TE mode coupling, there is no ATS.)

In the CPC case, output is also observed on the polarization orthogonal to the input polarization; fitting this output to a model allows us to find the nonreciprocity in CPC, i.e., the ratio of amplitudes $b = t_{21}/t_{12}$, as discussed elsewhere [13]. In the MSIT–MSIA case, output is also observed on the orthogonal polarization, which in this case is at -45° . This indicates that there is now coupling between the 45° and -45° superpositions. These effects are modeled, simulated numerically, analyzed theoretically, and confirmed experimentally. The results are presented here. We begin with the model including CPC and then simplify to the case applicable to MSIT and MSIA.

II. MODEL, SIMULATION, AND THEORY

We use a ring cavity model as shown in Fig. 1 to study the dynamics of CPC in a fiber-coupled microresonator. In Fig. 1, the subscripts 1 and 2 refer to the two orthogonal polarizations. E_{fj} is the input amplitude of polarization j , and

$$E_{rj} = r_j E_{fj} + it_j E_{sj} \quad (1)$$

is the throughput amplitude of polarization j . E_{sj} is the intracavity mode amplitude just before output coupling. The input and output coupling coefficients are taken to be equal, as discussed in Ref. [8], and given by it_j , with $r_j^2 = 1 - t_j^2 = 1 - T_j$, where T_j is the outcoupling loss for mode j .

*atr@okstate.edu

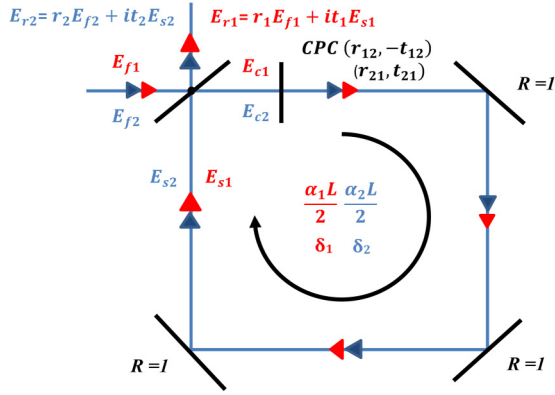


FIG. 1. Ring cavity representing tapered-fiber coupling to a microresonator with intracavity cross-polarization coupling. This figure is reproduced from Ref. [8].

In Fig. 1, δ_j and $\alpha_j L/2$ are the round-trip phase (modulo 2π) and intrinsic amplitude loss for mode j ; L is the resonator circumference; the intracavity mode amplitudes just after input coupling, E_{cj} , are not used in the analysis below. Cross-polarization coupling is represented in Fig. 1 as an effective intracavity wave plate and expressed by the coefficients $-t_{12}$ and t_{21} , where $t_{12}^2 = 1 - r_{12}^2$ and $t_{21}^2 = 1 - r_{21}^2$ are the polarization rotation probabilities per round trip, called T_s and T_p in Ref. [7].

The intracavity mode amplitudes E_{sj} satisfy the following time-evolution equations [8]:

$$\begin{aligned} \frac{d}{dt} E_{s1} &= -\gamma_1 E_{s1} - \frac{t_{12}}{\tau_{r1}} E_{s2} + \frac{it_1}{\tau_{r1}} E_{f1} - \frac{it_2 t_{12}}{\tau_{r1}} E_{f2}, \\ \frac{d}{dt} E_{s2} &= -\gamma_2 E_{s2} + \frac{t_{21}}{\tau_{r2}} E_{s1} + \frac{it_2}{\tau_{r2}} E_{f2} + \frac{it_1 t_{21}}{\tau_{r2}} E_{f1}. \end{aligned} \quad (2)$$

With these and Eq. (1), the time evolution of the throughput amplitudes can be found. In Eq. (2), $\tau_{rj} = n_j L/c$ is the round-trip time for mode j , where n_j is the effective refractive index of the mode, and

$$\gamma_j = \frac{T_j + \alpha_j L}{2\tau_{rj}} - i \frac{\delta_j}{\tau_{rj}} = \kappa_j (1 + i\theta_j), \quad (3)$$

with $\kappa_j = \frac{\omega_0}{2Q_j}$ being the amplitude decay rate, or half the inverse of the photon lifetime in mode j (both modes are resonant at ω_0), and θ_j being the offset of the resonant frequency of mode j from the input frequency in units of half the mode linewidth.

When there is input of only one polarization, we set $E_{f2} = 0$ and by taking the time derivative of Eq. (1) and using Eq. (2), we can model the throughput response to an input pulse. By solving Eq. (2) in steady state, we can model the throughput spectrum, CMIT being characterized by a dip with a central narrow peak and CMIA being characterized by a dip with a central narrower dip [8].

Equations (2) for the intracavity mode amplitudes are implicitly written in a frame rotating at ω_0 . In the nonrotating frame, and if there is no input so that γ_j becomes κ_j , the time-evolution operator for the intracavity mode amplitudes

in the TM-TE (1-2) basis becomes

$$\begin{pmatrix} -i\omega_0 - \kappa_1 & -\gamma_{12} \\ \gamma_{21} & -i\omega_0 - \kappa_2 \end{pmatrix}, \quad (4)$$

where $\gamma_{12} = t_{12}/\tau_{r1}$ and $\gamma_{21} = t_{21}/\tau_{r2}$. This matrix has eigenvalues

$$\lambda_{\pm} = -i\omega_0 - \kappa_{\pm} \pm \sqrt{\kappa_{-}^2 - \gamma_{21}\gamma_{12}},$$

$$\text{where } \kappa_{\pm} = \frac{1}{2}(\kappa_1 \pm \kappa_2). \quad (5)$$

These correspond to the two eigenvectors, which are the supermodes. Note that $\kappa_{-} \neq 0$ since we assume that $Q_1 \ll Q_2$ and hence $\kappa_1 \gg \kappa_2$. If the radicand is positive, the supermodes have the same frequency but different decay rates, and they are linearly polarized superpositions of TM and TE – this is the case of CMIT, where there is input on mode 1 only. However, these superpositions are not simply symmetric and antisymmetric, and the polarizations of the supermodes are not, in general, orthogonal. When the CPC strength is increased enough to make the radicand negative, the supermode frequencies split and their polarizations become elliptical – this is the case of ATS. The point of transition, where the radicand is zero, is the exceptional point, where not only the two eigenvalues, but also the two eigenvectors, coalesce into a single eigenvalue and a single eigenvector [14].

In contrast, for MSIT, a superposition of E_{s1} and E_{s2} that we will call E_{s+} is created by input light linearly polarized at 45° ($E_{f1} = E_{f2}$). We assume that there is no CPC, so the off-diagonal elements of the matrix of Eq. (4) are zero. That evolution matrix, in the basis that is the 1–2 basis rotated by 45° , then has the form

$$\begin{pmatrix} -i\omega_0 - \kappa_{+} & -\kappa_{-} \\ -\kappa_{-} & -i\omega_0 - \kappa_{+} \end{pmatrix}, \quad (6)$$

where the mode amplitudes forming the new basis are

$$E_{s\pm} = \frac{1}{\sqrt{2}}(E_{s1} \pm E_{s2}). \quad (7)$$

Now, even though there is no CPC between E_{s1} and E_{s2} , E_{s+} and E_{s-} will be coupled if $\kappa_{-} \neq 0$. Since, as in CMIT, we will assume that $Q_1 \ll Q_2$ or $\kappa_1 \gg \kappa_2$, this will be the case and this coupling gives rise to MSIT. The eigenvalues of the matrix of Eq. (6) are

$$\lambda_{\pm} = -i\omega_0 - \kappa_{+} \pm \kappa_{-}, \quad (8)$$

so there is no possibility of ATS; in fact, the supermodes are seen to be the original 1 and 2, i.e., TM and TE.

Now we can model the throughput spectrum and pulse response for MSIT and MSIA. Let the input mode amplitude be E_{f+} , defined in terms of E_{f1} and E_{f2} as in Eq. (7), and similarly the throughput mode amplitude is E_{r+} so that the input light is linearly polarized at 45° , and the throughput at 45° is detected. Since the difference in effective refractive indices of modes 1 and 2 is relatively small, we take them to have the same effective n , implying that the phase detunings can be taken to be equal, and so

$$\delta_1 = \delta_2 = \delta = \frac{2\pi nL}{c}(v - v_0) \quad (9)$$

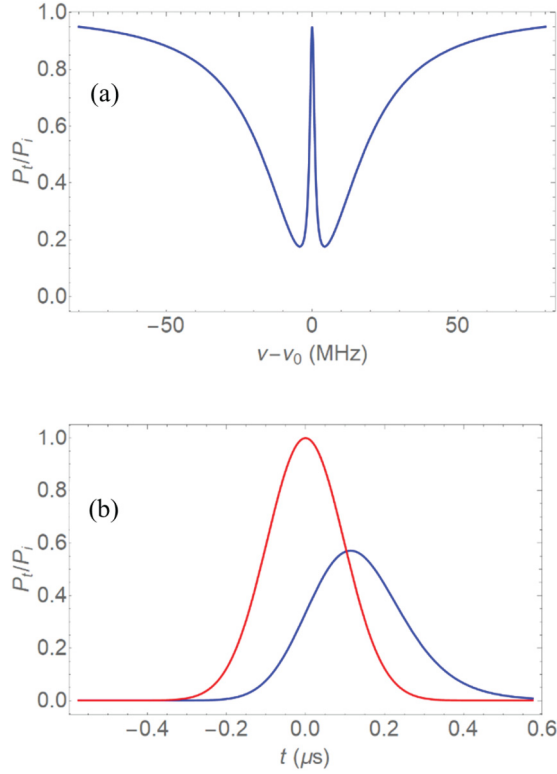


FIG. 2. (a) Simulated MSIT throughput spectrum. (b) Delayed output pulse (lower, blue) compared to the input pulse (upper, red). Assumed parameter values: $Q_1 = 5.0 \times 10^6$, $Q_2 = 1.0 \times 10^8$; $M_1 = 0.05$ (overcoupled), $M_2 = 0.05$ (overcoupled), $\Delta = 0.0$ MHz, $\Delta\tau_p = 230$ ns, $\Delta_p = 0.0$ MHz, $\Delta\nu_p = 1.92$ MHz.

gives the relation of δ to the frequency detuning from resonance, $\nu - \nu_0$, where $\nu_0 = \omega_0/2\pi$. Now set $t_{12} = t_{21} = 0$ in Eq. (2) and find the relative throughput to be given by

$$\frac{E_{r+}}{E_{f+}} = \frac{1}{2} \left[\frac{\alpha_1 L - T_1 - i2\delta}{\alpha_1 L + T_1 - i2\delta} + \frac{\alpha_2 L - T_2 - i2\delta}{\alpha_2 L + T_2 - i2\delta} \right]. \quad (10)$$

An example of a simulated MSIT throughput spectrum [the squared modulus of the expression in Eq. (10)] is shown in Fig. 2, along with the simulated Gaussian pulse response for the same parameter values. The width of the central peak (transparency window) is approximately the same as the linewidth of the higher- Q mode 2, and the throughput pulse is seen to be delayed and reduced in amplitude compared to the Gaussian input pulse.

The parameters involved in Fig. 2 include the quality factors of the modes, inversely proportional to the total loss,

$$Q_j = \frac{2\pi nL\nu}{c(T_j + \alpha_j L)} = \frac{\nu}{\Delta\nu_j}, \quad (11)$$

where $\Delta\nu_j$ is the WGM linewidth. The ratio of the outcoupling loss to the intrinsic loss is $x_j = T_j/\alpha_j L$; a mode is overcoupled if this ratio is greater than 1, and undercoupled if the ratio is less than 1. The fractional resonance dip depth of mode j is given by

$$M_j = \frac{4x_j}{(1+x_j)^2}. \quad (12)$$

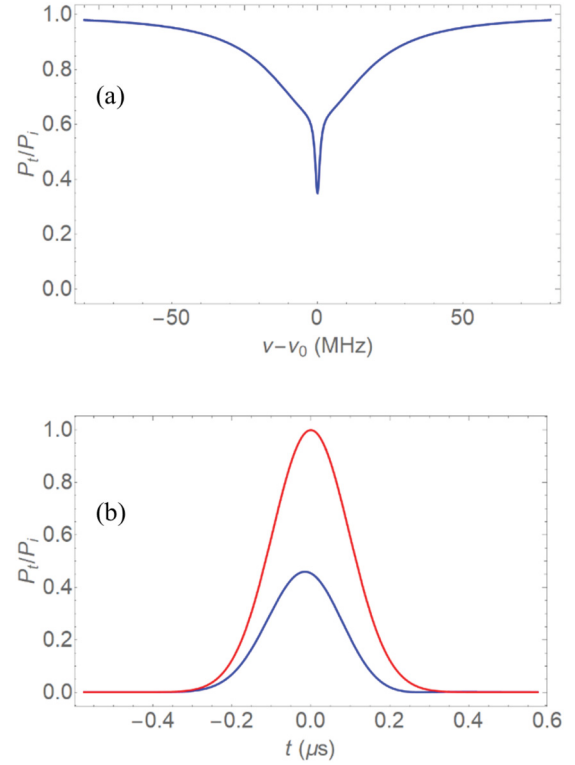


FIG. 3. (a) Simulated MSIA throughput spectrum. (b) Advanced output pulse (lower, blue) compared to the input pulse (upper, red). Assumed parameter values: $Q_1 = 5.0 \times 10^6$, $Q_2 = 1.0 \times 10^8$; $M_1 = 0.65$ (undercoupled), $M_2 = 0.65$ (undercoupled), $\Delta = 0.0$ MHz, $\Delta\tau_p = 230$ ns, $\Delta_p = 0.0$ MHz, $\Delta\nu_p = 1.92$ MHz.

Knowing Q_j , M_j , and the coupling regimes determines the values of T_j and $\alpha_j L$. The detuning from coresonance is $\Delta = \nu_2 - \nu_1$, where $\nu_1 = \nu_0$. The detuning of the pulse center frequency from ν_0 is Δ_p , and the input pulse width is $\Delta\tau_p$, corresponding to a pulse bandwidth of

$$\Delta\nu_p = \frac{2 \ln 2}{\pi \Delta\tau_p}. \quad (13)$$

The pulse width is chosen to be large enough that its frequency bandwidth is no greater than the width of the central peak or dip, which is roughly the range of steep dispersion. Figures 3 and 4 illustrate MSIA.

In Fig. 3, a simulated example of MSIA with pulse advancement is shown, and Fig. 4 is an example of MSIA with pulse delay. Again, just as in CMIA [8], different parameter values that result in MSIA can lead to advancement or delay of a resonant input pulse. A proof of this will be given below. The range of steep dispersion, that is, the width of the transparency or attenuation window, is essentially the same as the linewidth of mode 2, as mentioned above. This will now be shown for the special case of both modes strongly overcoupled.

The square modulus of Eq. (10) subtracted from 1 is analogous to the probe absorption spectrum in electromagnetically induced transparency (EIT) [15]. In the case of MSIT, when x_1 and x_2 are both large compared to 1 – both modes strongly

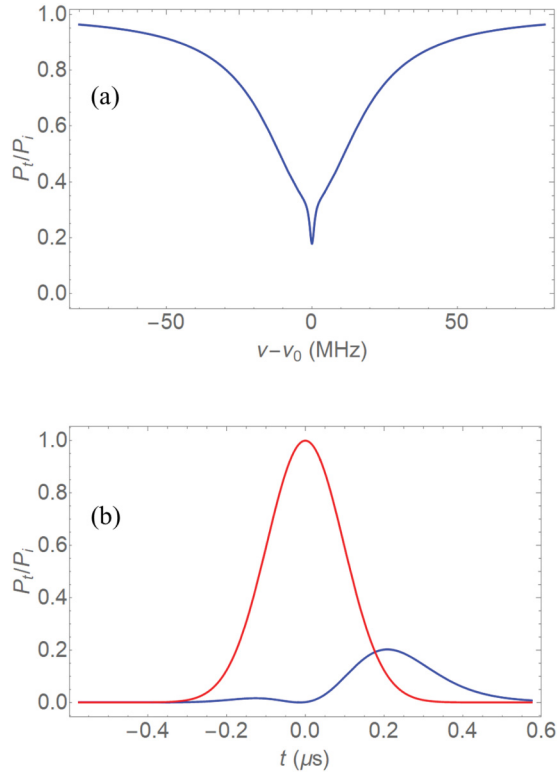


FIG. 4. (a) Simulated MSIA throughput spectrum. (b) Delayed output pulse (lower, blue) compared to the input pulse (upper, red). Assumed parameter values: $Q_1 = 5.0 \times 10^6$, $Q_2 = 1.0 \times 10^8$; $M_1 = 0.99$ (undercoupled), $M_2 = 0.13$ (overcoupled), $\Delta = 0.0$ MHz, $\Delta\tau_p = 230$ ns, $\Delta_p = 0.0$ MHz, $\Delta\nu_p = 1.92$ MHz.

overcoupled – this expression is

$$1 - \left| \frac{E_{r+}(\delta)}{E_{f+}} \right|^2 = \frac{\left(\frac{T_1}{2}\right)^2}{\left(\delta + \frac{T_1 T_2}{4\delta}\right)^2 + \left(\frac{T_1}{2}\right)^2}. \quad (14)$$

Comparison to a similar expression for EIT shows that the phase width of the central peak is T_2 , the linewidth (in phase) of mode 2. Note, however, that there is one significant difference; in similar expressions for EIT [15], coupled-resonator-induced transparency (CRIT) [16], and CMIT [8,17], the first term in the denominator has a minus sign rather than a plus sign. The effect of this sign change for MSIT is simply a reduction in the depth of the twin dips in Fig. 2(a).

To evaluate the delay or advancement of a pulse, write Eq. (10) in polar form, calling the phase ϕ ; then the throughput delay τ of an input pulse can be found from

$$\tau = \frac{nL}{c} \frac{d\phi}{d\delta} \Big|_{\delta=0} = \tau_{rt} \frac{d\phi}{d\delta} \Big|_{\delta=0}. \quad (15)$$

(Since we assume that modes 1 and 2 have the same effective index, they have the same round-trip time.) For MSIT or MSIA, without making any assumptions about the coupling regimes or the relative Q values of the two modes, the dispersion is found to be

$$\frac{d\phi}{d\delta} \Big|_{\delta=0} = 2 \frac{\frac{x_1^2}{T_1}(x_2 + 1)^2 + \frac{x_2^2}{T_2}(x_1 + 1)^2}{(x_1 + 1)(x_2 + 1)(x_1 x_2 - 1)}. \quad (16)$$

From Eq. (16), the value of $x_1 x_2$ determines whether a pulse will be delayed or advanced. If $x_1 x_2 > 1$, the pulse will be delayed; if $x_1 x_2 < 1$, the pulse will be advanced. The simulations of Figs. 2–4 all assume a resonator radius of $300 \mu\text{m}$, so the delays in those three examples are 1.3×10^4 , -2.3×10^3 , and 2.4×10^4 round-trip times, respectively.

To investigate the throughput spectrum, use Eq. (3) to rewrite Eq. (10) as

$$\left| \frac{E_{r+}}{E_{f+}} \right| = \frac{1}{2} \left| \frac{\frac{1-x_1}{1+x_1} + i\theta_1}{1+i\theta_1} + \frac{\frac{1-x_2}{1+x_2} + i\theta_2}{1+i\theta_2} \right|. \quad (17)$$

What is measured will be the square of this, i.e., the ratio of throughput intensity or power to input intensity or power, as shown in Figs. 2(a), 3(a), and 4(a). Keep in mind that θ_j is the frequency detuning from resonance in units of the linewidth of mode j . Our usual condition that $Q_1 \ll Q_2$ means that mode 2 has a much narrower linewidth than mode 1. Thus, it is possible to have a detuning such that $\theta_1 \ll 1 \ll \theta_2$. At this detuning, the throughput will be just outside the central peak or dip; comparing Eq. (17) evaluated at this detuning to its evaluation at zero detuning will determine whether we have MSIT (greater at zero) or MSIA (less at zero). At zero, $\theta_1 = \theta_2 = 0$, and

$$\left| \frac{E_{r+}}{E_{f+}} \right| = \frac{|1 - x_1 x_2|}{(1 + x_1)(1 + x_2)}, \quad (18)$$

whereas, when $\theta_1 \ll 1 \ll \theta_2$,

$$\left| \frac{E_{r+}}{E_{f+}} \right| = \frac{1}{1 + x_1} = \frac{1 + x_2}{(1 + x_1)(1 + x_2)}. \quad (19)$$

To have pulse advancement, the numerator of Eq. (18) will be $1 - x_1 x_2$, which can never be greater than $1 + x_2$ [the numerator of Eq. (19)], so advancement is only possible in MSIA. For delay, the numerator is $x_1 x_2 - 1$, which can be greater than or less than $1 + x_2$, so delay can occur in both MSIT and MSIA.

Note that the throughput pulses in Figs. 2–4 are broadened and slightly distorted with respect to the input pulses. This is a consequence of choosing the pulse width such that the delay or advancement is an appreciable fraction of the pulse width. In these cases, both the phase ϕ and the group delay τ of Eq. (15) vary over the pulse bandwidth, as illustrated in Fig. 5.

From the numerical model, the phase ϕ of the throughput spectra in Figs. 2–4 is calculated and plotted, and the group delay $\tau = d\phi/d\omega$ is found and plotted. The input pulse's Gaussian frequency spectrum is also plotted along with ϕ and τ . In each case, there is variation of the phase and delay over the pulse bandwidth, explaining the distortion and broadening of the throughput pulse.

Because the extent of the spectral region of steep dispersion is determined by the linewidth of the higher- Q mode, this system is not optimized for broadband pulse delay, unlike systems that make use of multiple resonances [18]. Our purpose here is just to show that delay and advancement occur, and to specify the conditions for those occurrences.

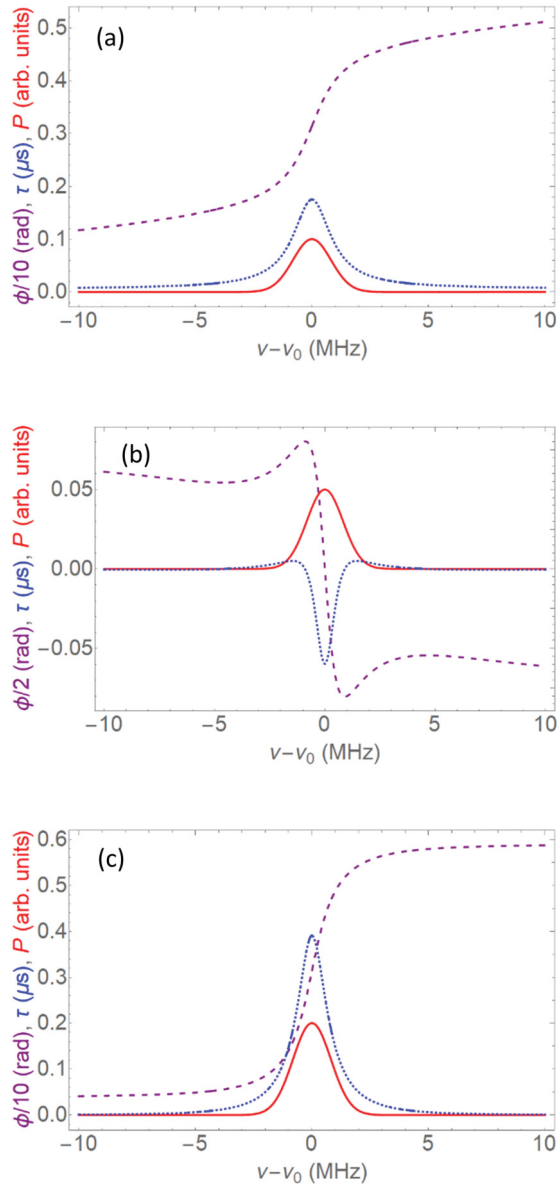


FIG. 5. Throughput phase ϕ (dashed purple), group delay τ (dotted blue), and pulse wave-packet P (solid red) vs frequency. (a) Corresponds to the case of Fig. 2, (b) to Fig. 3, and (c) to Fig. 4.

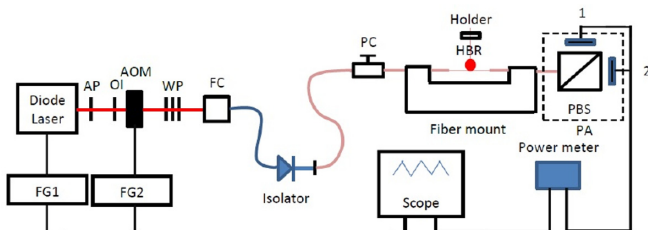


FIG. 6. Experimental setup. This figure is reproduced from Ref. [8].

III. EXPERIMENTAL RESULTS

To determine the CPC strength in CMIT and ATS, we used an experimental setup as shown in Fig. 6. The same setup is now used to investigate MSIT and MSIA.

The tunable diode laser (1550-nm wavelength) is scanned in frequency and its free-space beam passes through an acousto-optic modulator. Wave plates and a compression-based polarization controller are used to control the input polarization. The coupling fiber is made adiabatically bitapered and brought into contact with the hollow-bottle resonator (HBR) in its equatorial plane using a 3D translation stage (not shown). The HBR is mounted on a piezo-controlled holder for strain tuning. A more detailed description of the HBR can be found elsewhere [7,19,20]. The length of fiber after the HBR is kept short and straight to preserve the polarization.

In all cases, the resonator is kept inside an acrylic box to minimize temperature fluctuations and other effects of air movement. The output signal is sent to a polarization analyzer (PA), which includes a polarizing beam splitter (PBS) plus two detectors and can be rotated about the fiber axis so that either detector can detect either polarization. For data analysis, the detector signals are separately input to the oscilloscope.

Light polarized at 45° in the TM-TE basis is input, the HBR is strain-tuned to TE-TM coresonance, and the throughput spectrum of the input polarization (the PA is rotated about the fiber axis by 45° from the orientation shown in Fig. 6) is observed. An MSIT or MSIA feature is observed when the laser is scanned; for the pulse response, the laser is tuned to resonance. Individual mode parameters are measured [8] by tuning away from coresonance and using input of the two polarizations sequentially. Those parameters are, for mode j : quality factor Q_j , relative throughput dip depth M_j , and the coupling regime. In addition, the mistuning from coresonance Δ and the detuning of the pulse center frequency from resonance Δ_p are estimated. Using those parameters (there are no free parameters), the model is compared to the experimental spectral trace. The width of the Gaussian input pulse is measured and input to the model to predict the throughput pulse.

Figures 7–9 show three typical examples that correspond qualitatively to the simulations of Figs. 2–4: MSIT with pulse delay, MSIA with pulse advancement, and MSIA with pulse delay. In Figs. 7–9, note that the experimental pulse identified as the input pulse is actually a throughput pulse measured far off resonance. The experimental delay and advancement ranges between $3.4 \times 10^3 \tau_{rt}$ and $9.4 \times 10^3 \tau_{rt}$. However, the agreement between experiment and model is not perfect. There is qualitative agreement, but the form of the experimental throughput spectrum is not matched perfectly by the model, and the delay and height of the throughput pulse are also imperfectly predicted by the model.

Although constrained by the lack of any truly free parameters, adjustment of the model was done in attempts to produce a better reproduction of the experimental results. The model assumes zero cross-polarization coupling, so some CPC was added back in, but this did not help. The detunings Δ and Δ_p are only estimated in the experiment, so these parameters were varied over reasonable ranges in the model, but to no avail. The coupling regime, which is found by touching a tapered

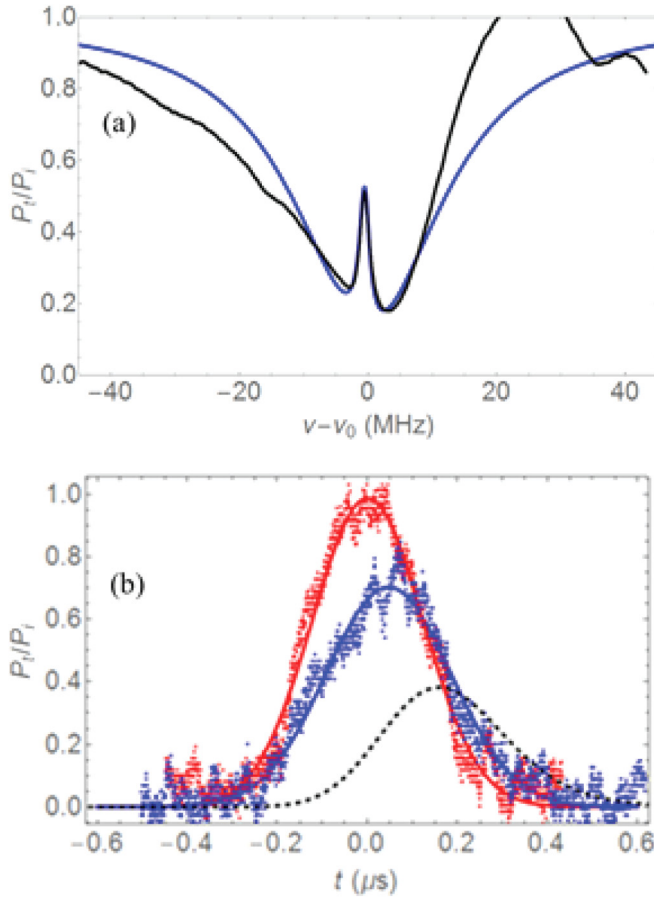


FIG. 7. MSIT with 170- μm -radius HBR. (a) Experimental (black) and model (blue) throughput spectra. (b) Experimental input (upper, red) and throughput (lower, blue) pulses, fitted by Gaussians, with a delay of 47 ns, and model throughput pulse (dashed black), with a delay of 150 ns. Parameter values: $Q_1 = 6.9 \times 10^6$, $Q_2 = 1.0 \times 10^8$; $M_1 = 0.61$ (overcoupled), $M_2 = 0.32$ (overcoupled), $\Delta = -0.5$ MHz, $\Delta\tau_p = 285$ ns, $\Delta_p = -0.5$ MHz, $\Delta\nu_p = 1.55$ MHz.

fiber to the other side of the resonator to effectively increase the intrinsic loss, can sometimes be difficult to determine with certainty, but changing it in the model did not help. The individual mode quality factors and dip depths were also varied slightly in the model, and the input polarization and the orientation of the polarization analyzer in the model were adjusted a bit as well. None of these tactics resulted in significantly better quantitative agreement between the experiment and the model.

This inability to improve the quantitative agreement suggests that the model, which assumes one TE mode and one TM mode, is incomplete. Since the input light has both TE and TM components, modes of both polarization families are being excited. This makes it more difficult to achieve coresonance between a well-isolated TE WGM and a well-isolated TM WGM. It is easier in CMIT, when the input is of a single polarization [8,9]. Inspection of the experimental throughput spectra in Figs. 7–9 suggests that the main reason for quantitative disagreement is spectral overlap with modes other than the main two coresonant WGMs. This can

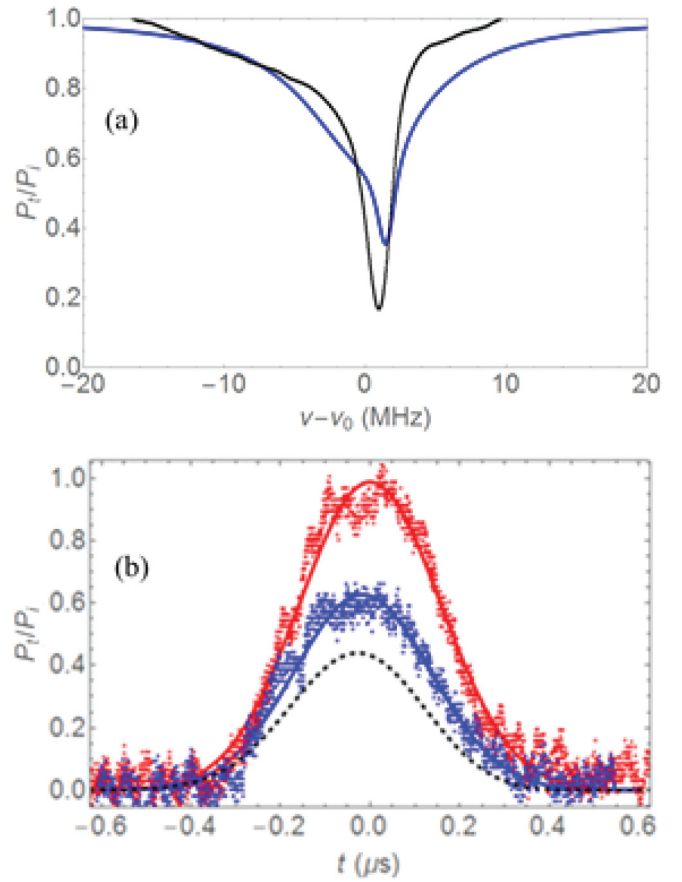


FIG. 8. MSIA with 170- μm -radius HBR. (a) Experimental (black) and model (blue) throughput spectra. (b) Experimental input (upper, red) and throughput (lower, blue) pulses, fitted by Gaussians, with an advancement of 17 ns, and model throughput pulse (dashed black), with an advancement of 25 ns. Parameter values: $Q_1 = 1.8 \times 10^7$, $Q_2 = 1.2 \times 10^8$; $M_1 = 0.69$ (undercoupled), $M_2 = 0.64$ (undercoupled), $\Delta = 1.5$ MHz, $\Delta\tau_p = 370$ ns, $\Delta_p = 1.3$ MHz, $\Delta\nu_p = 1.19$ MHz.

explain not only discrepancies in the throughput spectra, but also the throughput pulse height and delay disagreements, because the throughput pulse is shown relative to the input pulse. If the input pulse's height is changed and/or it is delayed because of the effect of another mode when measuring the throughput pulse off resonance, both the relative height and delay of the resonant throughput pulse can be affected.

IV. CONCLUSIONS

This work advances the examination of polarization effects in whispering-gallery microresonators; superposition of uncoupled coresonant WGMs having orthogonal polarizations and very different Q s is studied theoretically and modeled numerically. The results of this analysis show that it is possible for the throughput to show MSIT, with pulse delay, and MSIA, with pulse advancement or delay. Experimental investigation confirms these results; MSIT with pulse delay has been observed, as in Fig. 7, and MSIA with pulse advancement and

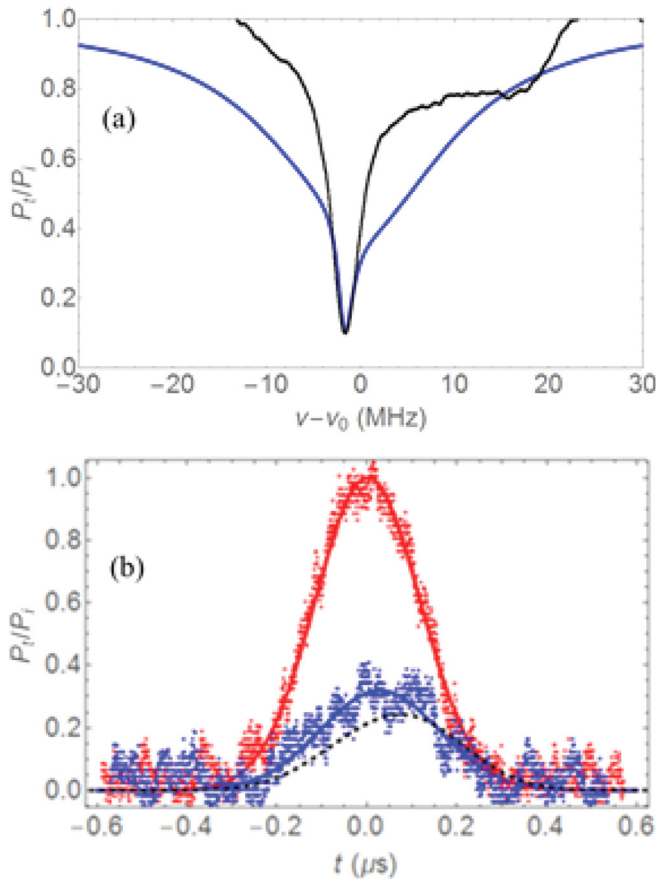


FIG. 9. MSIA with 170- μ m-radius HBR. (a) Experimental (black) and model (blue) throughput spectra. (b) Experimental input (upper, red) and throughput (lower, blue) pulses, fitted by Gaussians, with a delay of 27 ns, and model throughput pulse (dashed black), with a delay of 70 ns. Parameter values: $Q_1 = 8.4 \times 10^6$, $Q_2 = 1.0 \times 10^8$; $M_1 = 0.96$ (undercoupled), $M_2 = 0.23$ (overcoupled), $\Delta = -1.8$ MHz, $\Delta\tau_p = 275$ ns, $\Delta_p = 0.0$ MHz, $\Delta\nu_p = 1.60$ MHz.

MSIA with pulse delay have also both been observed, as in Figs. 8 and 9, respectively. Comparison of experimental results to the model predictions given the experimental parameter values (no free parameters) shows qualitative agreement. Reasonable partial fits to the experimental throughput spectra are found, but the experimental and modeled amplitude and delay (or advancement) of the throughput pulse differ quantitatively, as illustrated in Figs. 7–9.

The most likely cause of the quantitative disagreement between experiment and model is spectral mode overlap. The potential excitation of TM and TE modes other than the co-resonant two that form the desired superpositions is an effect not accounted for in the model. This spectral mode overlap can affect both the throughput spectra and the relative height and delay of the throughput pulse.

In the experiment, mode overlap can be reduced by using an HBR with a different bulge profile, and carefully positioning a somewhat thicker tapered fiber with respect to it. Experimental reduction of mode overlap is preferable to extending the model to account for additional modes. Such an extended model would likely introduce unwanted free parameters, as it would be difficult to completely characterize the additional modes in an experiment.

In general, any application for which induced transparency (or attenuation) is suited could potentially benefit from using MSIT rather than CMIT, since CPC is not required. For example, preliminary investigations suggest that MSIT could provide a sensitivity enhancement over CMIT if used for dissipative sensing. With the analyte inside the HBR, only the WGM with the higher radial order will interact with it, if the lower-radial-order WGM does not have an internal fraction. This can change the shape of the throughput spectrum, in particular the height of the central peak.

Throughout this work, the model assumed that there was no CPC. Also, the experimental cases that were studied were selected to be those showing no evidence of CPC. However, the effects on MSIT of having some residual CPC warrant further study.

-
- [1] H. Konishi, H. Fujiwara, S. Takeuchi, and K. Sasaki, Polarization-discriminated spectra of a fiber-microsphere system, *Appl. Phys. Lett.* **89**, 121107 (2006).
- [2] S. Ramelow, A. Farsi, S. Clemmen, J. S. Levy, A. R. Johnson, Y. Okawachi, M. R. E. Lamont, M. Lipson, and A. L. Gaeta, Strong polarization mode coupling in microresonators, *Opt. Lett.* **39**, 5134 (2014).
- [3] Y.-C. Liu, B.-B. Li, and Y.-F. Xiao, Electromagnetically induced transparency in optical microcavities, *Nanophotonics* **6**, 789 (2017).
- [4] M. N. M. Nasir, S. B. Gorajoobi, G. S. Murugan, and M. N. Zervas, Polarization effects in optical microresonators, *J. Opt. Soc. Am. B* **36**, 705 (2019).
- [5] J. Kreissmann and M. Hentschel, Spin-orbit interaction of light in three-dimensional microcavities, *Phys. Rev. A* **102**, 043524 (2020).
- [6] C. Wang, X. Jiang, W. R. Sweeney, C. W. Hsu, Y. Liu, G. Zhao, B. Peng, M. Zhang, L. Jiang, A. D. Stone, and L. Yang, Induced transparency by interference or polarization, *Proc. Natl. Acad. Sci. USA* **118**, e2012982118 (2021).
- [7] A. T. Rosenberger, E. B. Dale, K. V. Bui, E. K. Gonzales, D. Ganta, L. Ke, and S. R. Rajagopal, Cross-polarization coupling of whispering-gallery modes due to the spin-orbit interaction of light, *Opt. Lett.* **44**, 4163 (2019).
- [8] K. V. Bui and A. T. Rosenberger, Coupled-mode-induced transparency and attenuation resulting from cross-polarization coupling, *Phys. Rev. A* **101**, 033836 (2020).
- [9] L. Ke, S. R. Rajagopal, and A. T. Rosenberger, Dynamical determination of the strength of cross-polarization coupling in a whispering-gallery microresonator, *Phys. Rev. A* **104**, 053534 (2021).

- [10] M. R. Foreman, J. D. Swaim, and F. Vollmer, Whispering gallery mode sensors, *Adv. Opt. Photon.* **7**, 168 (2015).
- [11] W. Yoshiki, Y. Honda, T. Tetsumoto, K. Furusawa, N. Sekine, and T. Tanabe, All-optical tunable buffering with coupled ultra-high Q whispering gallery mode microcavities, *Sci. Rep.* **7**, 10688 (2017).
- [12] D. D. Smith, H. Chang, K. Myneni, and A. T. Rosenberger, Fast-light enhancement of an optical cavity by polarization mode coupling, *Phys. Rev. A* **89**, 053804 (2014).
- [13] K. Sandoval, M. Junaid Ul Haq, and A. T. Rosenberger, Asymmetric cross-polarization coupling between microresonator whispering-gallery modes, *Proc. SPIE* **12016**, 120160D (2022).
- [14] M.-A. Miri and A. Alù, Exceptional points in optics and photonics, *Science* **363**, eaar7709 (2019).
- [15] M. Fleischhauer, A. Imamoglu, and J. P. Marangos, Electromagnetically induced transparency: Optics in coherent media, *Rev. Mod. Phys.* **77**, 633 (2005).
- [16] D. D. Smith, H. Chang, K. A. Fuller, A. T. Rosenberger, and R. W. Boyd, Coupled resonator induced transparency, *Phys. Rev. A* **69**, 063804 (2004).
- [17] A. T. Rosenberger, Comparison of methods for achieving induced transparency or absorption with pulse delay or advancement in a single microresonator, *Proc. SPIE* **9763**, 97631E (2016).
- [18] O. Tsilipakos, L. Zhang, M. Kafesaki, C. M. Soukoulis, and T. Koschny, Experimental implementation of achromatic multiresonant metasurface for broadband pulse delay, *ACS Photonics* **8**, 1649 (2021).
- [19] R.-I. Stoian, K. V. Bui, and A. T. Rosenberger, Silica hollow bottle resonators for use as whispering gallery mode based chemical sensors, *J. Opt.* **17**, 125011 (2015).
- [20] R.-I. Stoian, B. K. Lavine, and A. T. Rosenberger, pH sensing using whispering gallery modes of a silica hollow bottle resonator, *Talanta* **194**, 585 (2019).